ChemComm

A Benzoquinone-Derived Porous Hydrophenazine Framework for Efficient and Reversible Iodine Capture

Journal:	*ChemComm*
Manuscript ID	CC-COM-09-2018-007529.R1
Article Type:	Communication

Journal Name

COMMUNICATION

A Benzoquinone-Derived Porous Hydrophenazine Framework for Efficient and Reversible Iodine Capture

Received 00th January 20xx,
Accepted 00th January 20xx

DOI: 10.1039/x0xx00000x

www.rsc.org/

Kecheng Jie,[a,b] Hao Chen,[a] Pengfei Zhang,[b,c] Wei Guo,[a,b] Meijun Li,[a] Zhenzhen Yang,[a] and Sheng Dai*[a,b]

A type of benzoquinone-derived porous organic polymer with hydrophenazine linkages, porous hydrophenazine frameworks, were developed. Their application in iodine capture from both air and solution was investigated.

Porous organic polymers (POPs) are a fascinating class of materials with the features of high surface areas, synthetic diversity, low densities, and great thermal/chemical stabilities.[1-4] In light of these unique advantages, there has been rapid development of POPs to explore their wide applications in catalysis, separations, gas storage, environmental treatment, and so on.[5-8] To fabricate stable POPs, it is typically necessary to use rigid building blocks (repeating units) to prevent the collapse of the framework and fill the volume space in a more periodic manner. The rigidity of POPs is normally based on the rigid repeating aromatic units.[1-8] Meanwhile, the chemical bonds that connect the lightweight aromatic units should also be rigid enough to avoid framework shrinkage.

Chemists and materials scientists have applied numerous organic synthetic strategies to form rigid chemical bond linkages in the synthesis of POPs. To date, these have been mostly realized by polymerization or polycondensation through C–X (X=C, O, N) bond formation strategies, such as metal-mediated couplings, oxidative coupling, imine/amide/imide-based condensation, aromatic nucleophilic substitution, radical polymerization, cyclotrimerization, hyper-crosslinking processes by Lewis acids, and so on.[9-16] Benefiting from these processes, the chemistry of POPs have been greatly expanded and the targeted engineering of POPs with specific requirements related to surface area, pore size, surface affinity, and target functional group have been successfully achieved. Given the abundance of organic synthetic procedures, the exploration of new synthetic strategies to construct POPs with simple building blocks is still meaningful to enrich the POP class with unique functions.

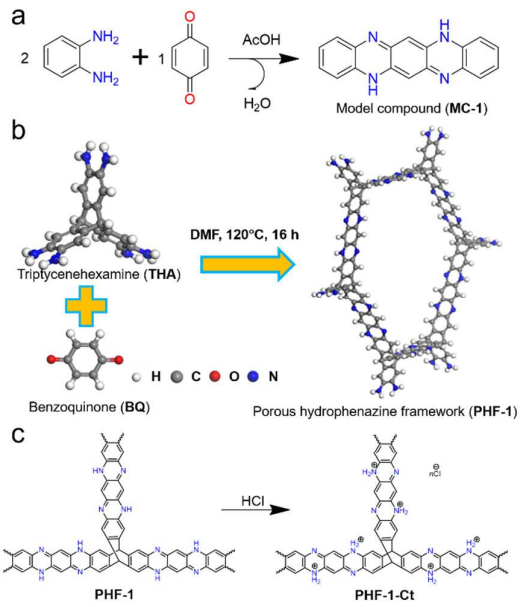

Scheme1. (a) The synthetic procedure of a model compound (**MC**) using *o*-phenylenediamine and benzoquinone (**BQ**). (b) The illustration of the synthesis of a porous hydrophenazine framework (**PHF-1**) using triptycenehexamine (**THA**) and **BQ** *via* a solvothermal Method. (c) Synthesis of cationic **PHF-1-Ct** by protonation of **PHF-1** with diluted HCl.

In this study, we developed a novel class of POPs with hydrophenazine linkages. Derived from benzoquinone (**BQ**) and triptycenehexamine (**THA**), porous hydrophenazine frameworks (**PHFs**) were successfully synthesized *via* a catalyst-free aza-ring formation reaction between *ortho*-diamine and **BQ** (Scheme 1a and 1b).[17] To the best of our knowledge, such a synthetic strategy has never before been used in the synthesis of POPs. The preparation of **PHFs** did not require strict reaction conditions (an anhydrous and oxygen-free environment) or catalysts and took only a few hours to complete the reaction. The resultant neutral **PHF** (**PHF-1**) had a high Brunauer-Emmett-Teller (BET) specific surface area (1046 m^2/g) as well as good thermal and physiochemical stability. The nitrogen-rich

a Department of Chemistry, The University of Tennessee, Knoxville, TN, 37996, USA. E-mail: dais@ornl.gov.
b Oak Ridge National Laboratory, Oak Ridge, TN 37831, USA.
c School of Chemistry and Chemical Engineering, Shanghai Jiaotong University, Shanghai 200240, China.
Electronic Supplementary Information (ESI) available: [details of any supplementary information available should be included here]. See DOI: 10.1039/x0xx00000x

PHF-1 also displayed an exceptional CO_2 adsorption capacity. Furthermore, the neutral **PHF-1** was easily protonated with dilute hydrochloride (HCl) to become positively charged **PHF-1-Ct** because of the existence of aniline groups on the hydrophenazine rings. The protonation resulted in a decrease in the BET surface area and the CO_2 adsorption capacity. Intriguingly, the positively charged **PHF-1-Ct** with lower BET surface area displayed an efficient iodine capture capacity (4.05 g/g) higher than that of the neutral **PHF-1** (3.05 g/g) and was the highest among the amorphous POPs.[18-24] The higher iodine loading amount in **PHF-1-Ct** was ascribed to the multiple binding sites for both neutral iodine molecules and polyiodide anions. Moreover, the **PHFs** were recycled many times without losing their iodine capture ability.

We began the study with the synthesis of an aza-fused hydrophenazine-like model compound (**MC-1**) using *o*-phenylenediamine and **BQ**. The 2:1 reaction with **BQ** dropwise added into the *o*-phenylenediamine solution afforded **MC-1** with a yield of over 95% within 30 min (Scheme 1a, Fig. S4–S7).[17] Thus, an effficient rigid-ring formation reaction may be suitable for the synthesis of POPs. Replacing *o*-phenylenediamine with **THA**, a rigid threefold symmetric building block, resulted in a 2-dimensional (2D) shape-persistent hydrophenazine-linked framework with inherent periodic honeycomb-like structures (**PHF-1**) after a solvothermal reaction. The yield of the polymeric product was increased from 30% to 88% by an extension of the reaction time from 8 to 16 h (Scheme 1b). The **PHF-1** polymer network was chemically stable and was insoluble in common organic solvents such as DMF, acetone, and alcohols.

The structure of **PHF-1** was first characterized by solid state ^{13}C cross-polarization magic-angle spinning (CP/MAS) nuclear magnetic resonance (NMR) at the molecular level (Fig. 1a). The solid-state ^{13}C CP-MAS NMR spectrum revealed eight carbon peaks with chemical shifts of 52.8, 80.6, 113.3, 122.4, 132.9, 140.6, 170, and 201.9 ppm, which were assigned to the sp^3 bridge carbon (a), the aromatic (sp^2) carbons (b, d, e, f, g, h), and the edge carbonyl (C=O) groups (c), respectively (Fig. 1a). X-ray photoelectron spectroscopy (XPS) was performed to probe the nitrogen bonding nature in **PHF-1** (Fig. 1b). The peaks at 398.78 eV and 400.28 eV were attributed to the characteristic imine nitrogen atoms and aniline nitrogen atoms,[25] respectively, revealing the formation of hydrophenazine rings in the **PHF-1** structure (Fig. 1b). The Fourier-transform infrared spectrum showed several peaks at 3345 cm^{-1}/3180 cm^{-1}, 2160 cm^{-1}, 1186 cm^{-1}/1210 cm^{-1}, and 1620 cm^{-1}, corresponding to the stretching vibrations of N-H, C=N, and C-N and the in-plane bending vibrations of N-H, respectively (Fig. 1c). This was in good agreement with the XPS results. Thermogravimetric analysis (TGA) showed an apparent weight loss began at temperatures as high as 580 °C, indicating the high thermal stability of **PHF-1** (Fig. 1d).

To investigate the long-range ordering of the **PHF-1** structure, a powder x-ray diffraction (PXRD) experiment was performed. No sharp peaks were observed in the PXRD spectrum, indicating the loss of long-range crystallographic ordering of **PHF-1** (Fig. S10). The bulk morphologies of **PHF-1** were visualized with field-emission scanning electron microscopy (FE-SEM). The SEM images showed that **PHF-1** consisted of relatively uniform solid sub-micron spheres (Fig. 1e and 1f). These fused polymer masses without well-defined shapes also implied the loss of long-range order. The fluffy sample may be favourable for good porosity, especially the mesoporosity or macroporosity that exists among the micro-spheres.

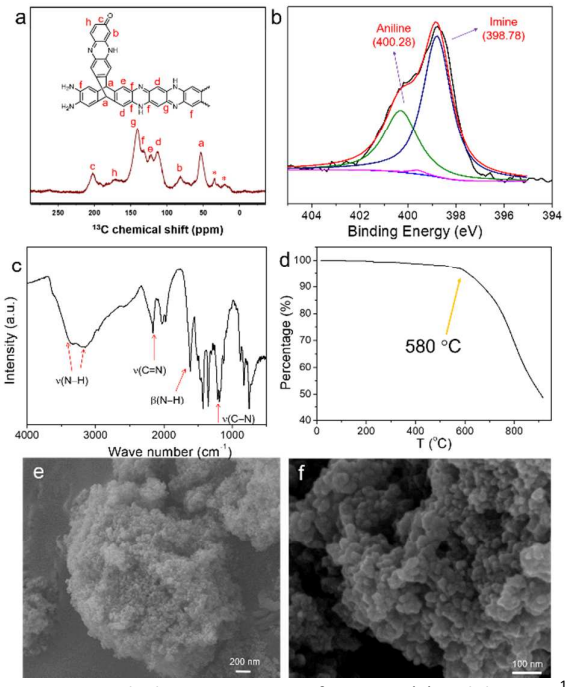

Fig. 1. Structural characterization of **PHF-1**: (a) Solid state ^{13}C-CP/MAS NMR spectrum. The asterisk denotes spinning sidebands. (b) N 1s XPS spectrum. (c) Fourier-transform infrared spectrum. (d) TGA curve of the as-prepared sample of **PHF-1** under a nitrogen atmosphere after in situ activation at 150 °C in a TGA instrument to remove any adsorbed guest molecules. (e), (f) Field-emission scanning electron microscope images at different scales.

Interestingly, our initial findings showed that **MC-1** was protonated by diluted HCl to become positively charged **MC-1-Ct** owing to the presence of aniline groups in the structure. This was confirmed from the disappearance of the proton signals on aniline groups in the ^1H NMR spectrum (Fig. S9). Thus, the protonation of **PHF-1** afforded positively charged **PHF-1** (**PHF-1-Ct**). The structure of **PHF-1-Ct** was characterized by ^{13}C CP-MAS NMR, Cl 2p XPS, and SEM. The ^{13}C CP-MAS NMR spectrum of **PHF-1-Ct** was very similar to that of **PHF-1** (Fig. S11), indicating the integrity of **PHF-1-Ct** after protonation. FE-SEM images also displayed that **PHF-1-Ct** had a similar morphology to **PHF-1** (Fig. S12). The Cl 2p XPS spectrum showed a peak at 198.78 eV (Fig. S13), corresponding to the chloride anions, thus confirming the formation of positively charged **PHF-1-Ct** with chloride counterions.

The porosity of both **PHF-1** and **PHF-1-Ct** was investigated by nitrogen adsorption-desorption experiments at 77 K. In Fig. 2a, typical type II sorption isotherms can be observed for both **PHF-1** and **PHF-1-Ct**, indicating the irregular pore sizes within these two materials. The remarkable N_2 uptake below P/P_0 = 0.1 can be ascribed to micropores within the expanded frameworks of the 2D rigid building blocks, whereas the increasing N_2 uptake at P/P_0 > 0.9 may be related to the textural large meso/macropores formed by interstitial voids (Fig. 2a). The BET surface area of the neutral **PHF-1** was calculated to be 1046 m^2/g with a total pore volume of 0.61 cm^3/g. However, the calculated BET surface area of cationic **PHF-1-**

Ct was 690 m^2/g with a total pore volume of 0.44 cm^3/g—lower than that of **PHF-1**. We deduced that the presence of chloride anions in **PHF-1-Ct** led to a decrease in the accessible pores for N_2. Meanwhile, the level of microporosity was assessed by the ratio of micropore volume to the total pore volume (V_{micro}/V_{total}).[26] The V_{micro}/V_{total} values of **PHF-1** and **PHF-1-Ct** were 0.57 and 0.59, respectively, indicating the good microporosity of the two porous polymers (Table 1).

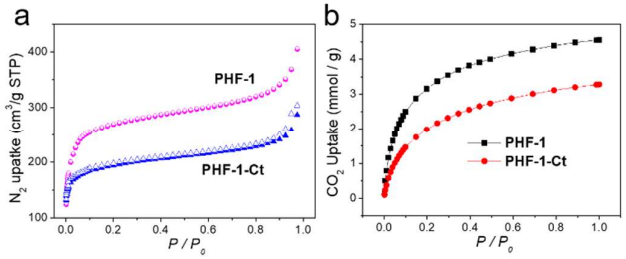

Fig. 2. (a) N_2 adsorption and desorption isotherms at 77 K and (b) CO_2 adsorption isotherms of **PHF-1** and **PHF-1-Ct** at 273 K.

The two nitrogen-rich porous materials also showed superb CO_2 uptake capacities. Uptakes of 4.55 mmol/g (20.0 wt %) and 3.28 mmol/g (14.4 wt %) at 1 bar and 273 k were obtained for **PHF-1** and **PHF-1-Ct**, respectively (Fig. 2b). The results revealed that **PHF-1** with a larger BET surface area had a better CO_2 capture performance than **PHF-1-Ct** with a lower BET surface area. Moreover, the CO_2 uptake in **PHF-1** was comparable to that of many reported POPs.[26] The reason can be ascribed to the synergistic effects of rich microporosity and abundant CO_2-philic surface sites, including unreacted peripheral C=O sites and nitric sites.[27,28]

Table 1. Porosity Parameters of PHFs

PHFs	SA_{BET} (m^2/g)	V_{total} (cm^3/g)	V_{micro} (cm^3/g)	V_{micro}/V_{total}
PHF-1	1046	0.61	0.35	0.57
PHF-1-Ct	690	0.44	0.26	0.59

Radiological iodine species such as ^{129}I and ^{131}I are common nuclear volatile fission wastes formed during the production of nuclear power.[29-31] They need to be efficiently captured and reliably stored. The two **PHFs**, with their features of good porosity, high electron density, and abundant aromatic/aza rings may also have exceptional iodine capture capabilities. To explore this question, iodine vapor adsorption experiments were first performed. Fig. S14 shows that the colors of both **PHF-1** and **PHF-1-Ct** became darker after adsorption of iodine vapor. This phenomenon indicated that iodine molecules were not only adsorbed onto the surface but also loaded into the intrinsic pores of the two porous polymers. Iodine uptake capacities were measured by gravimetric methods that depend on the differences of sample weights before and after exposure to iodine vapor. Upon reaching equilibrium, one gram of **PHF-1-Ct** and **PHF-1** adsorbed approximately 4.05 g and 3.05 g of iodine, respectively (Fig. 3a). TGA results showed that the weight losses below 300 °C of **PHF-1-Ct** and **PHF-1** after adsorption of iodine were 80% and 75%, respectively, corresponding to the iodine capture capacity of 4.0 g/g and 3.0 g/g (Fig. S15 and S16). The results thus agreed well with gravimetric measurements. It was worth noting that the iodine loading capacity of **PHF-1-Ct** was the highest among the POPs and the second-highest among all reported materials (Table S1).[18-24] SEM images showed that iodine-loaded **PHF-1** consisted of large nanoparticles, whereas iodine-loaded **PHF-1-Ct** consisted of nanorods, both of which were different from their original morphologies (Fig. S17). This implied that the mesopores or macropores between the small spheres of **PHF-1** or **PHF-1-Ct** were filled with iodine, resulting in the morphology change. It should be mentioned that **PHF-1-Ct**, with a lower BET surface area, had a better iodine capture performance than **PHF-1** with a higher BET surface area, which was contrary to the CO_2 capture results. The mechanism behind this result was verified by XPS. Iodine species adsorbed in **PHF-1** with only a valence of zero were detected, confirming that iodine remained as neutral I_2 (Fig. 3b). This finding revealed a purely physical adsorption process of iodine in **PHF-1**. However, iodine species of both neutral I_2 and polyiodide anion I_3^- were detected in **PHF-1-Ct**, indicating that some adsorbed iodine molecules were transformed to I_3^- by **PHF-1-Ct** (Fig. 3c). Moreover, the positively charged nitrogen-fused aromatic **PHF-1-Ct** produced multiple supramolecular interactions with iodine, such as typical charge transfer interactions between phenyl rings and iodine molecules,[23,31] N – H···I halogen bonding interactions,[23] and electrostatic interactions between positively charged ammonium group and I_3^-, thereby increasing the adsorption amount for iodine.

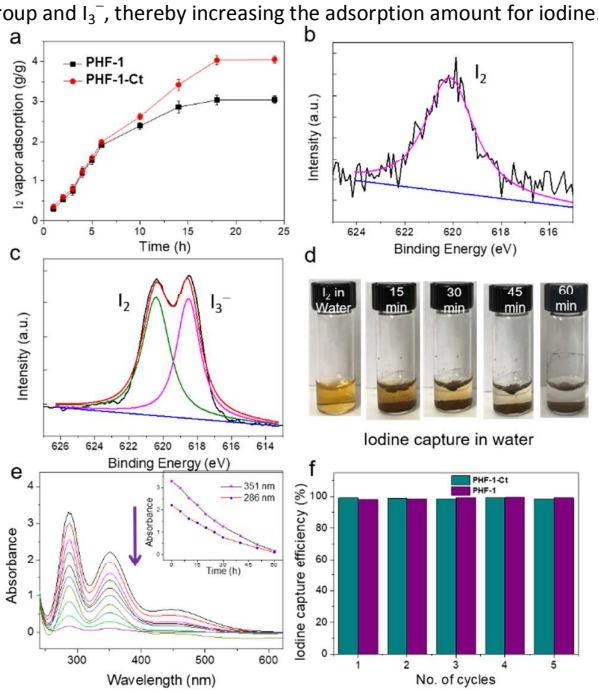

Fig. 3. (a) Time-dependent iodine vapor capture capacities of **PHF-1** and **PHF-1-Ct**. I 3d XPS spectra: (b) **PHF-1** and (c) **PHF-1-Ct** after capture of iodine vapor. (d) Photographs and (e) time-dependent UV/vis absorption spectra when 25 mg of **PHF-1-Ct** were placed in 2 mL iodine aqueous solution. (f) Iodine capture efficiency after **PHF-1** and **PHF-1-Ct** were recycled five times.

PHF-1-Ct was also able to capture iodine dissolved in solution. Upon the addition of **PHF-1-Ct** to an iodine *n*-hexane solution, the purple solution faded over time and turned completely colorless after 60 minutes (Fig. S18a). A time-dependent ultraviolet–visible spectroscopy (UV/Vis)

experiment (Fig. S18b) showed that the iodine concentration decreased over time to nearly zero after 120 min. This means that **PHF-1-Ct** captured iodine from *n*-hexane with a final concentration of iodine below 1 ppm. Moreover, **PHF-1-Ct** was capable of capturing iodine in aqueous solution, which has only rarely been demonstrated by porous materials, such as metal-organic frameworks, because of their moisture instability (Fig. 3d). It also took about 60 min to completely adsorb iodine in a saturated aqueous iodine solution, a somewhat faster rate than that in *n*-hexane (Fig. 3e).

To be practically useful, an adsorbent should be reused over multiple cycles without loss of performance. When iodine-loaded **PHF-1** or **PHF-1-Ct** was exposed to ethanol, the transparent solvent soon became yellow, indicating the spontaneous release of iodine (Fig. S19). After being immersed in ethanol for 5 hours, the **PHFs** were collected, washed with ethanol, and dried for the next use. The recovered **PHFs** were still able to capture iodine without an apparent loss of iodine loading capacity after five cycles (Fig. 3f).

In conclusion, we for the first time employed a catalyst-free aza-ring formation reaction between **BQ** and *ortho*-diamines to prepare a novel class of porous organic polymers with hydrophenazine linkages—**PHFs**. The neutral **PHF-1** had a higher BET surface area and CO_2 adsorption capacity. However, the positively charged **PHF-1-Ct** with a lower BET surface area displayed an efficient iodine capture capacity that was higher than that of the neutral **PHF-1** and was the highest among all reported amorphous POPs. The high iodine loading capacity of **PHF-1-Ct** was ascribed to the multiple binding sites for both neutral iodine molecules and polyiodide anions. Compared with other iodine adsorbents, **PHFs** have several advantages beside their high loading capacity. For example, the preparation of **PHFs** from **BQ** is extremely simple and cost-effective. Moreover, because of their moisture and thermal stability, **PHFs** can capture not only volatile iodine in the air but also iodine dissolved in organic and aqueous solutions. Finally, they can be reused many times without an apparent loss in performance. Given the abundance of building blocks containing diamines or **BQ**s, various **PHFs** will be developed *via* this synthetic method for targeted applications in the near future. Particular interest may be focused on the construction of hydrophenazine-linked crystalline covalent organic frameworks.

Conflicts of interest

There are no conflicts to declare.

ACKNOWLEDGMENT

This work was supported by the Division of Chemical Sciences, Geosciences, and Biosciences, Office of Basic Energy Sciences, US Department of Energy.

Notes and references

1 S. Das, P. Heasman, T. Ben and S. Qiu, *Chem. Rev.*, 2017, **117**, 1515.
2 A. G. Slater and A. I. Cooper, *Science*, 2015, **348**, 988.
3 C. S. Diercks and O. M. Yaghi, *Science*, 2017, **355**, 923.
4 Cooper, A. I. *ACS Cent. Sci.*, 2017, **3**, 544.
5 J. R. Li, R. Kuppler and H.-C. Zhou, *Chem. Soc. Rev.*, 2009, **38**, 1477.
6 J. Reboul, S. Furukawa, N. Horike, M. Tsotsalas, K. Hirai, H. Uehara, M. Kondo, N. Louvain, O. Sakata and S. Kitagawa, *Nat. Mater.*, 2012, **11**, 717.
7 D. Wu, F. Xu, B. Sun, R. Fu, H. He and K. Matyjaszewski, *Chem. Rev.*, 2012, **112**, 3959.
8 L. Ma, C. Abney and W. Lin, *Chem. Soc. Rev.*, 2009, **38**, 1248.
9 T. Ben, H. Ren, S. Ma, D. Cao, J. Lan, X. Jing, W. Wang, J. Xu, F. Deng, J. M. Simmons, S. Qiu and G. Zhu, *Angew. Chem. Int. Ed.*, 2009, **48**, 9457.
10 G. Zhang, Z.-A. Lan and X. Wang, *Angew. Chem. Int. Ed.*, 2016, **55**, 15712.
11 S. N. Talapaneni, T. H. Hwang, S. H. Je, O. Buyukcakir, J. W. Choi and A. Coskun, *Angew. Chem. Int. Ed.* 2016, **55**, 3106.
12 J. Roeser, D. Prill, M. J. Bojdys, P. Fayon, A. Trewin, A. N. Fitch, M. U. Schmidt and A. Thomas, *Nat. Chem.*, 2017, **9**, 977.
13 H. Li, Q. Pan, Y. Ma, X. Guan, M. Xue, Q. R. Fang, Y. Yan, V. Valtchev and S. Qiu, *J. Am. Chem. Soc.*, 2016, **138**, 14783.
14 G. V. Bertrand, T. C. Ong and R. G. Griffin, *Proc. Natl. Acad. Sci. USA*, 2013, **110**, 4923.
15 J. X. Jiang, F. Su, A. Trewin, C. D. Wood, N. L. Campbell, H. Niu, C. Dickinson, A. Y. Ganin, M. J. Rosseinsky, Y. Z. Khimyak and A. I. Cooper, *Angew. Chem. Int. Ed.*, 2007, **46**, 8574.
16 Y. Xu, S. Jin, H. Xu, A. Nagai and D. Jiang, *Chem. Soc. Rev.*, 2013, **42**, 8012.
17 H. Kour, S. Paul, P. P. Singh and R. Gupta, *Synlett*, 2014, **25**, 495.
18 Z. Yan, Y. Yuan, Y. Tian, D. Zhang and G. Zhu, *Angew. Chem. Int. Ed.*, 2015, **54**, 12733.
19 Y. Liao, J. Webers, B. M. Mills, Z. Ren and C. F. J. Faul, *Macromolecules*, 2016, **49**, 6322.
20 F. Ren, Z. Zhu, X. Qian, W. Liang, P. Wu, H. Sun, J. Liu and A. Li, *Chem. Commun.*, 2016, **52**, 9797.
21 Y. Zhu, Y.-J. Ji, D.-G. Wang, Y. Zhang, H. Tang, X.-R. Jia, M. Song, G. Yu and G.-C. Kuang, *J. Mater. Chem. A*, 2017, **5**, 6622.
22 D. Shetty, J. Raya, D. S. Han, Z. Asfari, J.-C. Olsen and A. Trabolsi, *Chem. Mater.*, 2017, **29**, 8968.
23 Y. Lin, X. Jiang, S. T. Kim, S. B. Alahakoon, X. Hou, Z. Zhang, C. M. Thompson, R. A. Smaldone and C. Ke, *J. Am. Chem. Soc.*, 2017, **139**, 7172.
24 P. Wang, Q. Xu, Z. Li, W. Jiang, Q. Jiang and D. Jiang, *Adv. Mater.*, 2018, 1801991.
25 J.-B. Wu, Lin, Y.-F. Wang, J. Chang, P.-J. Tasi, C.-P. Lu, C.-C. Chiu, H.-T. Y.-W. Yang, *Inorg. Chem.*, 2003, **42**, 4516.
26 X. Zhu, C. Tian, T. Jin, K. L. Browning, R. L. Sacci, G. M. Veith and S. Dai, *ACS Macro Lett.*, 2017, **6**, 1056.
27 X. Zhu, C. Tian, G. M. Veith, C. W. Abney, J. Dehaudt and S. Dai, *J. Am. Chem. Soc.*, 2016, **138**, 11497.
28 X. Zhu, S. M. Mahurin, S.-H. An, C.-L. Do-Thanh, C. Tian, Y. Li, L. W. Gill, E. W. Hagaman, Z. Bian, J.-H. Zhou, J. Hu, H. Liu and S. Dai, *Chem. Commun.*, 2014, **50**, 7933.
29 F. C. Kuepper, M. C. Feiters, B. Olofsson, T. Kaiho, S. Yanagida, M. B. Zimmermann, L. J. Carpenter, G. W. Luther, Z. Lu, M. Jonsson and L. Kloo, *Angew. Chem. Int. Ed.* **2011**, *50*, 11598.
30 A. Saiz-Lopez, J. M. C. Plane, A. R. Baker, L. J. Carpenter, R. von Glasow, J. C. G. Martin, G. McFiggans and R. W. Saunders, *Chem. Rev.*, 2012, **112**, 1773.
31 K. Jie, Y. Zhou, E. Li, Z. Li, R. Zhao and F. Huang, *J. Am. Chem. Soc.*, 2017, **139**, 15320.